THE ASTROPHYSICAL JOURNAL, 505:443–451, 1998 September 20

X-RAY PHOTOELECTRON SPECTROSCOPY AND MASS SPECTROMETRY STUDIES OF X-RAY–PROCESSED SOLID CO_2

D. M. CORNELISON,[1] T. R. DILLINGHAM, S. C. TEGLER, K. GALLE, G. A. MILLER, AND B. L. LUTZ
Department of Physics and Astronomy, Northern Arizona University, P.O. Box 6010, Flagstaff, AZ 86011; david.cornelison@nau.edu, randy.dillingham@nau.edu, steve.tegler@nau.edu, miller@bohr.phy.nau.edu, barry.lutz@nau.edu
Received 1997 September 4; accepted 1998 April 21

ABSTRACT

Solid CO_2 films have been grown on a stainless steel substrate and processed by X-ray bombardment for up to 6 hr.. The reactions induced were monitored using X-ray photoelectron spectroscopy (XPS) and mass spectrometry. The XPS results are twofold: direct X-ray photolysis of the CO_2 ice produced CO and an unidentified O product, possibly atomic O; secondary effects resulting from surface reactions between CO, O, and residual H from the vacuum environment produced H_2CO, CH_3OH, and a water ice cap on the CO_2 film. The rate of production of CO from direct X-ray photolysis of CO_2 is measured to be 5.4×10^2 molecule photon^{-1}, corresponding to a formation cross section of 4.7×10^{-20} cm^2. The growth rate for the water cap is calculated to be 2.6×10^{-4} monolayers s^{-1} for a partial pressure of H equal to 2×10^{-10} Torr. The appearance of gas-phase products from the film showed a time lag which indicates that the diffusion of the product species in the bulk CO_2 is affected by some time-dependent process, possibly the creation of defects in the film. A model for the observed time dependence of the dissociation products in the gas phase yields diffusion coefficients in the CO_2 of 5×10^{-12} and 1×10^{-12} cm^2 s^{-1}, for O and CO, respectively.

Subject headings: diffusion — ISM: molecules — molecular processes — X-rays: general

1. INTRODUCTION

Understanding the chemical and material properties of ices (the term "ice" as used in this context refers to the solid phase of materials typically thought of as either liquids or gases) has become increasingly important in the astronomical community in recent years. Observational results over the last 20 years have shown that a large variety of molecules exist in the solid phase on dust grains in the interstellar medium (Allamandola et al. 1992; Blake et al. 1987 Lacy et al. 1991; Tielens et al. 1991; Turner 1990). H_2O is generally the most abundant, but nontrivial amounts of other molecules such as CO, H_2CO, and CH_3OH are also well established. In addition, many of these molecules have also been seen in comet comae and most likely exist in the solid phase within the cometary nucleus (see review by Mumma, Weissman, & Stern 1993).

For CO_2 ice specifically, its existence in the solid state within dust clouds has been generally accepted, even though earlier observational verification was a difficult task (d'Hendecourt & Jourdain de Muizon 1989). More recent work has confirmed its existence definitively in molecular clouds with an abundance larger than previously thought (deGraauw et al. 1996; Gürtler et al. 1996).

To better understand the abundances and detailed composition of these interstellar ices, various laboratories have initiated a core of experimental work in which the primary goal has been to create astronomically relevant ice mixtures in the lab and to observe the changes in the ice resulting from radiative processing by either UV photon (d'Hendecourt et al. 1986; Allamandola & Sandford 1988; Allamandola, Sandford, & Valero 1988) or MeV ion (Benit, Bibring, & Rocard 1988; Moore et al. 1983; Moore & Hudson 1992; Pirronello et al. 1982) bombardment. These efforts have met with a great deal of success and have generated useful data for comparison with observational spectra, especially in the IR (d'Hendecourt & Allamandola 1986; d'Hendecourt et al. 1986; Sandford & Allamandola 1990a, 1990b).

Some aspects of processed ices still remain relatively unexplored: first, in most previous work CO_2 has been studied as part of a mixture, of which it is usually a minor component. Gerakines, Schutte, & Ehrenfreund (1996) have recently processed several pure ices, including CO_2, with UV, proposing reaction pathways and measuring production cross sections, but more work should be done on pure ices to facilitate a thorough understanding of ice mixtures.

Second, the radiative processing of ices to initiate reactions of astronomical interest has almost exclusively been done using ultraviolet photons or MeV ions. Either is appropriate for most circumstances since there is a significant flux in interstellar dust clouds for both types of radiation. However, a case can be made to use X-rays as the processing radiation; for example, during the T Tauri phase of star formation, both classical and weak T Tauri stars emit in the X-ray wavelength region, with luminosities between 10^{29} and 10^{31} ergs cm^{-2} s^{-1} (Feigelson et al. 1993). Over the typical lifetime of this phase (about 1×10^6 yr) the dust grains surrounding these stars can undergo a significant amount of processing. Although the same direct chemistry may be seen when using X-rays instead of UV or MeV ions as the processing radiation, quantities such as production rates should differ, and the much higher energy of the X-rays compared to the UV may produce secondary effects not seen in the case of UV bombardment.

Third, theoretical efforts, which have concentrated on modeling the time dependence of gas- and solid-phase molecular abundances (d'Hendecourt, Allamandola, & Greenberg 1985; Hasegawa, Herbst, & Leung 1992; Tielens & Hagen 1982), suggest that surface reactions must be incorporated into current models to adequately explain

[1] Correspondence should be addressed to this author.

observations. For example, the abundance of H_2 in dust clouds depends on solid state chemistry, due to the need for a third body in the associative reaction between two H atoms (Hollenbach & Salpeter 1970, 1971; Pirronello et al. 1997). Surface reactions are also considered as sources for a great many other simple molecules (Greenberg et al. 1993; Williams 1993; Tielens 1992; Herbst 1993). Yet even though surface reactions are most certainly involved in the systems studied as part of astrochemistry, experimental surface science techniques have not typically been included in most studies. The probes used in previous work (such as IR spectroscopy) instead sample the entire ice volume and cannot easily detect surface effects.

To address these issues, we have begun work on the study of pure ices, irradiated by X-ray photons, and probed using the surface sensitive technique of X-ray photoelectron spectroscopy (XPS). Using this technique should provide details concerning the surface chemistry of the ices.

Because photoproduced species must reach the surface to initiate reactions, bulk diffusion will also play an important role in the surface physics of the ice. Unfortunately, very little work has been done on either the mechanisms or the kinetics of diffusion for these specific fragment/solid mixtures. The diffusion of various species in solid H_2O has been measured as a function of temperature and of other variables (Kopp, Barnaal, & Lowe 1965; Strauss, Chen, & Loong 1994), but similar data for solid CO_2 are scarce. Using a mass spectrometer to monitor the time dependence of the gas-phase molecular concentrations will enable us to learn something of the diffusion properties in the solid and will complement the XPS results.

In this paper, results are presented concerning the X-ray processing of a pure CO_2 ice grown under ultrahigh vacuum conditions. The details of the chemical changes that occur on the ice surface during the processing are investigated using the surface-sensitive technique of XPS. Furthermore, the gas-phase species evolved from the surface during the X-ray photoprocessing are monitored using a quadrupole mass spectrometer. Using these complementary techniques, a detailed picture of the reaction kinetics and a model concerning the diffusion of the X-ray photolysis products is given.

2. EXPERIMENT

High-quality ice films were grown on a stainless steel cold finger, cooled using a continuous flow liquid nitrogen system. Prior to film deposition, the stainless steel substrate was sputter cleaned for approximately 25 minutes using 4.0 keV Ar^+ ions. The CO_2 ice was formed from research grade (99.995% min purity) gas using a stainless steel gas nozzle placed directly over the cold finger. A baked, turbo-pumped manifold was used to input gas to the system, with partial pressures monitored using an MKS capacitance manometer. The base pressure in the chamber was less than 5×10^{-10} T prior to deposition and upon gas introduction was increased, using a precision leak valve, to approximately 5×10^{-8} T. The ice films were grown at this pressure for approximately 1 hr. This exposure resulted in a thickness of 5500 ± 825 Å. The thickness was measured by observing interference fringes on the ice as growth occurred. Upon introduction, the gas was monitored using a Balzers Prisma QMS 300 quadrupole mass spectrometer.

The ice films were characterized using the surface-sensitive technique of X-ray photoelectron spectroscopy (XPS). A general review of this technique can be found in Woodruff & Delchar (1994). The X-rays from the XPS source penetrate the entire sample since the attenuation of X-rays by solid CO_2 is small. However, the photoelectrons which are detected are severely attenuated, and the core level peaks result from the top 50–100 Å. The X-ray source was outgassed for 1 hr prior to the growth of the ice film, to reduce any background due to the source.

The XPS measurements were obtained using a PHI 5100 ESCA system equipped with a 27.9 cm hemispherical capacitor analyzer. The excitation source was Mg Kα radiation of energy 1253.6 eV. The reported photoelectron spectra were taken at a constant pass energy of 17.9 eV, which means the detector passes electrons of 17.9 eV only, requiring the photoelectrons to be decelerated before entering the analyzer. This technique maintains a constant resolution over the entire spectrum. All core level spectra were referenced to the C 1*s* line associated with a thin CO_2 ice film (growth for 1 minute at 5×10^{-8} T) on stainless steel. Under these conditions, charging effects for the ice were negligible. The C 1*s* line for this thin CO_2 ice film was observed at 292.75 eV, while the Fe $2p_{3/2}$ line associated with the stainless steel subtrate was observed before and after the deposition at 707.3 eV. It is noted that this reference binding energy for CO_2 ice is somewhat higher than the value of 292.1 eV reported previously by Gelius et al. (1970). For the spectra associated with X-ray–processed thick films, shifts in peak positions due to charging did occur. However, the relative spacing between C 1*s* and O 1*s* did not show any changes. Since the collection times were short compared to the irradiation times, no effort was made to keep the sample neutral, i.e., no electron bombardment of the sample was done. It should also be noted that the spectra are normalized, in all cases, to the height of the largest peak. This relative intensity scale will be discussed, where necessary, in the context of each spectrum.

Elemental stoichiometries were obtained from peak area ratios corrected by experimentally determined sensitivity factors. These stoichiometries are subject to uncertainties of $\sim 10\%$ of the stated value. The deconvolution of the XPS spectra was carried out using Gaussian component peaks with the constraint of having a nearly equal full width at half-maximum (FWHM) value for a given component among the different spectra.

The gas-phase species within the vacuum system were monitored during the growth phase of the ice using a Balzers QMS 300 quadruple mass spectrometer. The mass spectrometer was used in channeltron mode with the detector voltage set at 1200 V. The partial pressures were measured as ion currents, allowing relative comparisons between masses to be made. For some of the runs isotopic $^{13}CO_2$ was used to eliminate confusion between contributions to a mass number from more than one molecule. The multiple contributions are caused by the fractionation of the molecules by the mass spectrometer itself. During the X-ray processing of the ice, the mass spectrometer was operated continuously to monitor the species evolving from the surface. The XPS and mass spectrometer results are correlated and used to discuss the possible mechanisms associated with the photochemical processing of the ice.

We photoprocessed the ice using the X-ray source (Mg Kα at energy 1253.6 eV) of the XPS system, operated in a continuous mode. An X-ray photon of this energy will penetrate several microns of ice. The source was operated at 15

kV and 400 W and has a flux of 6×10^{13} photons cm^{-2} s^{-1} (E. Peterson 1997, private communication). Therefore, a total photon dose that may result in significant chemical changes in the laboratory experiment would occur on a very different timescale in an astrophysical environment. Effects such as diffusion and resurfacing, which are time dependent, may play a major role in the final result, and so caution should be taken when applying these results to astrophysical systems.

3. RESULTS

The chemical structure of the as-deposited and X-ray processed CO_2 ice was analyzed using XPS. From the line intensities of the detected elements and the corresponding sensitivity factors, we obtained the relative surface composition of the sample as a function of the X-ray–processing time. These results indicate that, for the initial ice, the total carbon to oxygen ratio is $\sim 1:2$, as expected. An increase in the oxygen concentration (with a corresponding decrease in the carbon concentration) is observed as the ice is processed using X-rays. After 6 hr, the ice has a carbon-to-oxygen ratio of $\sim 1:3$. Because of the surface sensitivity of XPS, this ratio does not necessarily reflect a change in the bulk concentrations, and the rise in the oxygen concentration is due to several processes which are discussed in detail below where the XPS and RGA results are presented.

The evolution of the C 1*s* core-level spectra is shown in Figure 1 for the CO_2 ice as a function of the X-ray–processing time. Figure 1*a* shows the initially grown ice with the main peak at 292.75 eV, which is associated with carbon in solid CO_2, as discussed previously. Figures 1*b* and 1*c* show the ice after X-ray photo-processing for 4 and 6 hr, respectively. In these figures, a tail is observed to grow on the low binding energy side of the main peak. Using standard line-shape analysis techniques, the tail was resolved using three distinct lines. These lines have been attributed to CO at 292.85 eV, H_2CO (formaldehyde) at 289.05 eV, and CH_3OH (methanol) at 287.78 eV. These energies were obtained from the literature (Siegbahn et al. 1969; Gelius et al. 1970) or from additional experiments on ice mixtures undertaken by this group. As an example, Figure 2*a* shows the C 1*s* core level for a CO_2/CH_3OH ice mixture. The lines are well resolved, and the spacing between the two peaks ($\Delta = 4.97$ eV) was used in the fit of Figure 1. We did not determine the mixing ratios for these calibration ices; only the spacing between lines was measured.

The O 1*s* core level spectra is shown in Figure 3 for the same data run as that of Figure 1. The as-grown ice is shown in Figure 3*a*, while Figures 3*b* and 3*c* show the 4 and 6 hr photoprocessed results. In the unprocessed case, the CO_2 line is placed at 536.32 eV. For the processed cases, a large tail is also seen to grow on the low binding energy side of the peak, while broadening occurs to higher binding energy. The tail and broadening were resolved by line-shape analysis using five distinct lines. These lines are attributed to CO at 537.52 eV, H_2CO at 535.50 eV, H_2O at 534.4 eV,

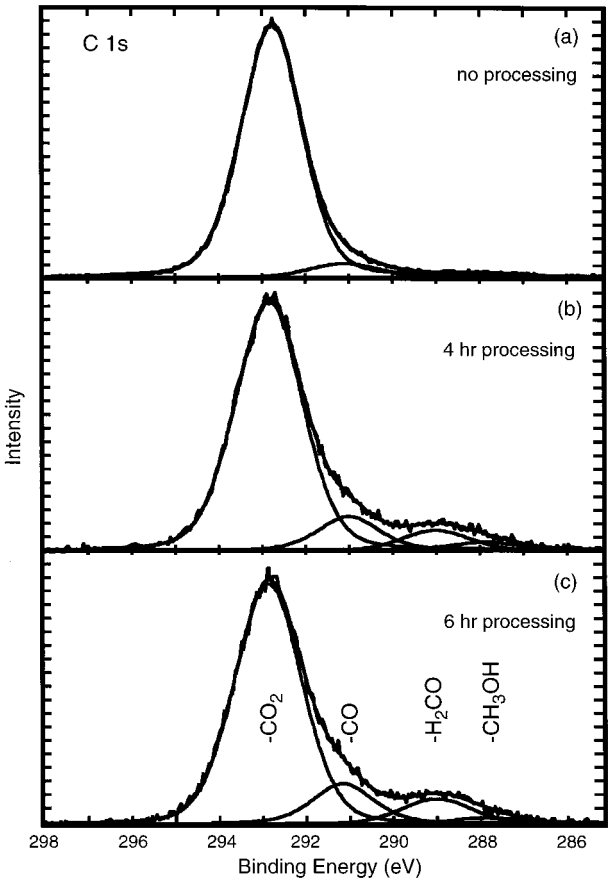

FIG. 1.—Time evolution of the C 1*s* core-level spectra for CO_2 ice during X-ray processing. The growth of CO, H_2CO, and CH_3OH is observed.

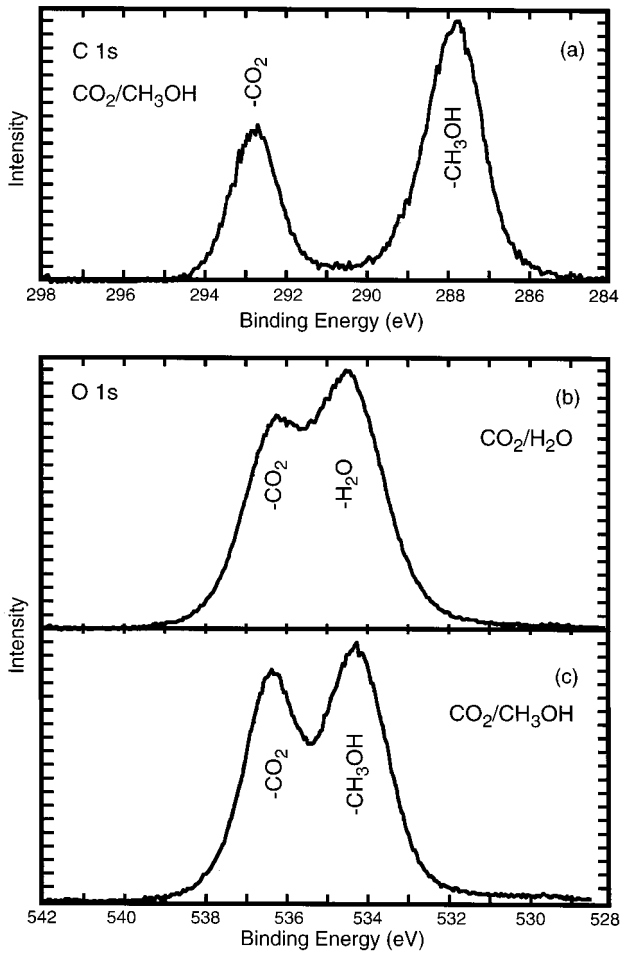

FIG. 2.—Core-level XPS spectra for determining line positions including (*a*) C 1*s* spectra for CO_2/CH_3OH ice mixture, (*b*) O 1*s* spectra for CO_2/H_2O mixture, and (*c*) O 1*s* spectra for CO_2/CH_3OH mixture.

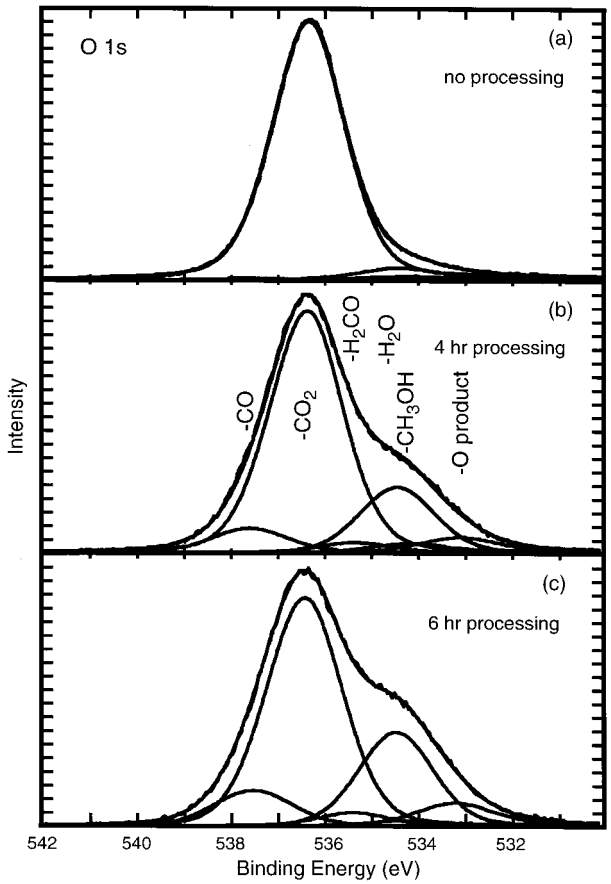

FIG. 3.—Time evolution of the O 1*s* core-level spectra for CO_2 ice during X-ray processing. The growth of CO, H_2CO, H_2O, CH_3OH, and trapped O is observed.

CH_3OH at 534.19 eV, and an additional O product at 533.1 eV. The energies for CO and H_2CO were determined from previous experimental work (Siegbahn et al. 1969; Gelius et al. 1970). The H_2O and CH_3OH energies were again directly measured. Figures 2*b* and 2*c* are plots of the O 1*s* core level spectra for CO_2/H_2O and CO_2/CH_3OH mixtures, respectively. Just as for the carbon line fits, the spacing between lines was used in the line-shape analysis.

Because of the large H_2O contribution in the spectra and the closeness of several of the lines, we set the amounts of the CO, H_2CO, and CH_3OH peaks by stoichiometric calculations using the results from the C 1*s* line-shape analysis. The data for the contribution of H_2O to the O 1*s* line were then fitted with constraints placed on line position and width, while the height was allowed to vary. To obtain a fit for the entire spectrum, while maintaining a reasonable line width for the H_2O, the additional line at 533.1 eV was needed. Since no other line accounts for the direct oxygen products of the X-ray induced photodissociation of the CO_2, it seems likely that this line is due to an oxygen-only molecule. The integrated intensity of the unidentified line is close to that of the CO contribution to the O 1*s*, and since for each photo-event one of each will be produced, this interpretation seems reasonable. Several candidates for this line are possible, specifically O, O_2, and O_3. UV-processing studies done on pure CO_2 ice suggest that the largest contribution to the products would come from O_3, although some O_2 would also exist (Gerakines et al. 1996). From this same work, the possibility of atomic O sitting in the matrix also seems to be less likely; once the ice was warmed to 30 K, atomic O diffused in the ice to form O_3. To our knowledge, little experimental data exist for the XPS line position for any of these oxygen molecules in the solid state. For now, we cannot unequivocally identify this contribution to the O 1*s* spectrum.

We also ran a control sample. The spectra for both the C 1*s* and O 1*s* lines in an unprocessed ice (5.2 hr after growth) are shown in Figures 4*a* and 4*b*, respectively. The amount of H_2O grown onto the ice surface from residual water in the vacuum is considerably less than during the processed run, as is seen by comparing Figures 3*c* and 4*b*, and noting the size of the H_2O contribution relative to the CO_2. The production of this H_2O from processing is also discussed below.

The evolution of dissociated constituents from the ice is best studied by monitoring the various mass species in the chamber as a function of time. Figure 5 is a plot of the relative gas pressures (as measured by ion current) for several masses as a function of time for a $^{13}CO_2$ ice. The processing began at $t = 0$ and continued until the moment marked by an arrow, at which time the X-rays were turned off to allow observation of the decay of species which were produced by the processing. Isotopic CO_2 was used so we could clearly distinguish masses for various constituents from background. These data preclude the possibility of evolution of gas due to heating of the ice from the X-ray source since the CO_2 (mass 45) pressure does not go up significantly throughout the entire experiment. In addition, we found that the masses which do show increases in pressure do so after a considerable time lag from the beginning of processing. This lag can be explained by more than one physical process, as is further discussed below.

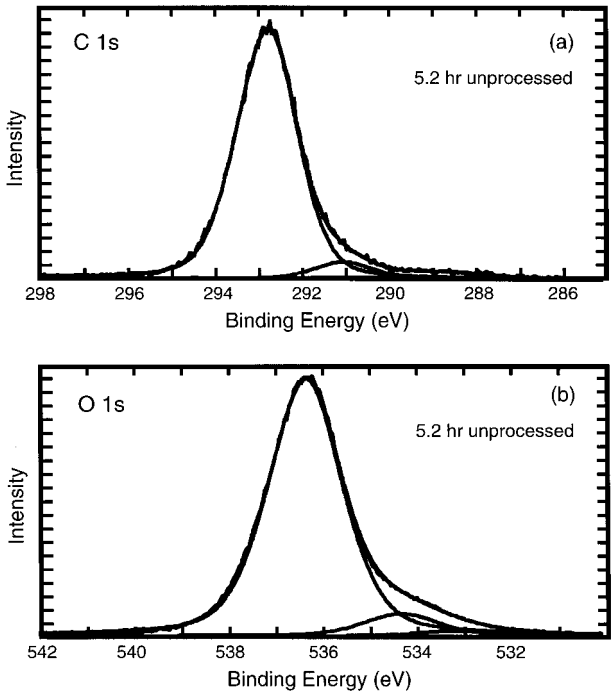

FIG. 4.—XPS spectra for unprocessed CO_2 ice 5.2 hr after growth showing (*a*) C 1*s* spectra and (*b*) O 1*s* spectra.

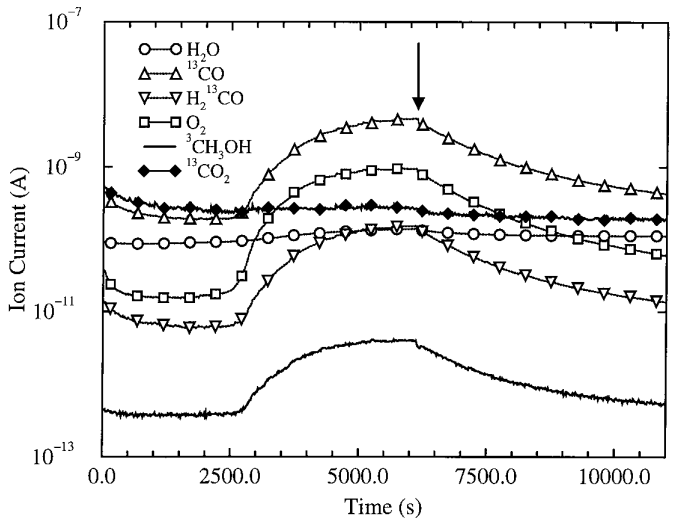

FIG. 5.—Time evolution of gas-phase concentrations for selected molecules in isotopic $^{13}CO_2$ ice. Processing began at $t = 0$ and was stopped at time indicated by arrow in order to observe decay of species in chamber.

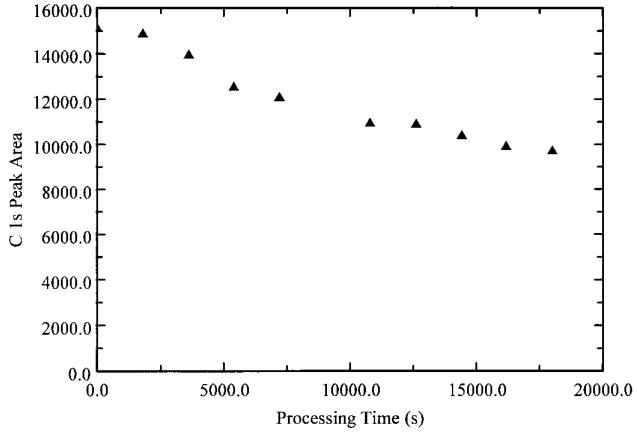

FIG. 6.—Total integrated area of C 1*s* XPS line as a function of processing time. Decrease in intensity can be modeled by exponential decay due to growth of photo-produced H_2O cap.

4. DISCUSSION

To fully understand the results of the X-ray processing, we must ultimately consider both bulk and surface characteristics. XPS is a surface sensitive technique and can probe processes which would be lost in the noise if the entire bulk were sampled On the other hand, this surface sensitivity can also give rise to misleading conclusions if one is also interested in bulk processes. Direct photolysis of the CO_2 by the X-ray flux should produce CO, O, and possibly C in the bulk of the ice. Our data show in Figures 1 and 3 that CO is indeed produced in the ice by the X-ray flux, and the mass spectrometer data in Figure 5 also confirm this conclusion. The data in Figure 5 also show an increase in mass 32, indicating that O_2 is also formed. Although not shown on the plot, an increase was also seen for mass 16; it unfortunately contains a large component due to the fractionation of CO and so is not shown. The rise in the chamber of mass 32 must result from some subsequent reaction since direct dissociation of CO_2 should lead to atomic O. Clearly, the data support the contention that we are producing both products of the photodissociation of the CO_2, so we have identifed the additional XPS O 1*s* peak at 533.1 eV as corresponding to O or O_2 trapped in the ice.

The photoproduced amount of each of these species is not readily determined, however, for several reasons. The produced species show a tendency to leave the ice film and enter the gas phase, but the absolute rates at which the species leave the ice is uncertain. The time at which large-scale diffusion from the ice begins is approximately 30 minutes. The XPS spectra were taken at either 30 minute or 1 hr intervals, and each spectra took about 10 minutes to complete. By the time we recorded the first XPS spectra after processing began, photoproduced species were already diffusing out of the CO_2, and, in some cases, equilibrium in the concentration of the species may have been reached. In addition to this diffusion, an H_2O cap grew on the CO_2 ice, as indicated by the decrease in the intensity of the C 1*s* line with time (Fig. 6) and the appearance of the H_2O signature in the O 1*s* spectra (Figs. 3*b* and 3*c*). this cap precludes using absolute intensities of the XPS lines as a measure of the production rate for the resultant species since the XPS technique samples only to a finite depth.

The integrated area of the XPS lines as a percentage of the C 1*s* total intensity would be a better indicator for the amount of each species existing within the ice, except that it still might not account for the total amount of each species produced over the duration of the experiment because of appreciable amounts lost to the gas phase. Using the amount of a species resident in the ice as a lower limit, we can, however, estimate the production rate for the X-ray photolysis of CO_2 to CO. The CO contribution to the total C 1*s* line after 6 hr is 6%, and, assuming the density of bulk CO_2 (1.56 g cm^{-3}) for the ice and a thickness of 5500 Å, we derive an X-ray photoproduction rate of 5.4×10^{-2} $photon^{-1}$, with an uncertainty of 20%. This rate corresponds to a formation cross section of 4.7×10^{-20} cm^2. Gerakines et al. (1996) found UV formation cross sections for CO in a CO_2 ice of 3.8×10^{-19} cm^2, and photoproduction rates for UV processing of various molecules were found to be of the same order of magnitude (d'Hendecourt et al. 1986). If we could include the amount of CO lost to the gas phase, the photoproduction rate would certainly rise. Later, we will make an estimate of this correction to improve the accuracy of this rate.

The X-ray processing also induced the formation of H_2CO and CH_3OH in the ice. The XPS spectra show clear growth for lines corresponding to both species. In the data from the mass spectrometer, we took care to distinguish contributions from H_2CO and CH_3OH because of the mass spectrometer's tendency to fractionate a portion of the molecules entering the analyzer. For example, H_2CO has a primary mass of 30, and CH_3OH of 32 amu. Consequently, fractionation of the CH_3OH will cause large signals at masses 32, 31, and 29, while for H_2CO, there will be large signals for masses 30, 29, and 28.

To eliminate any confusion, we repeated the experiment utilizing isotopic $^{13}CO_2$ in growing the ice. For $^{13}CO_2$, the masses are all shifted up one mass unit relative to $^{12}CO_2$ and give unequivocal correspondence of mass 31 to H_2CO and mass 33 to CH_3OH. In Figure 5, a rise in the mass corresponding to H_2CO and CH_3OH provides additional support that these species are both created during the X-ray processing of the CO_2 ice. Unlike CO and O, these products result from secondary reactions and rates for a multistep process have little meaning outside the specific experiment from which they were obtained. However, qualitative information about these two molecules can yield useful informa-

tion. Both H_2CO and CH_3OH molecules require that the CO and O produced from direct X-ray photolysis find hydrogen bearing species to react with. An important question is whether the hydrogenation reactions producing the secondary molecules occur in the bulk or on the surface of the ice. The UHV system in which the experiment was performed is an exceptionally clean environment. While great care was taken to ensure that the initial CO_2 ice was as pure as possible, other molecules are obviously present in the chamber, as in any vacuum system. In fact, the most abundant background species in a UHV chamber at 10^{-10} T pressure is hydrogen, in either molecular or atomic form. The level of H_2O, the most likely other hydrogen bearing molecule, in the chamber is 2 orders of magnitude below the level of CO_2 during deposition while the level of H is only a factor of 2 lower. Thus, some hydrogen could be trapped in the ice during growth. This trapped H (or H_2) would be available for photolysis and reaction with the CO and O fragments to form both H_2CO and CH_3OH in the bulk.

It is also possible that these molecules are formed via hydrogenation reactions occurring on the surface of the ice (Herbst 1993; Tielens 1992). In the UHV chamber, the partial pressure of the H_2 and H is approximately 2×10^{-10} T, which leads to hydrogen striking the surface of the ice at a rate of 1×10^{11} cm^{-2} s^{-1}. Calculations yield small values for the sticking probability for H or H_2 on an oxide surface for a lattice temperature of less than 100 K (Leitch-Delvin & Williams 1985), unless chemisorption sites are available. The surface in this case may have active chemisorption sites due to the constant X-ray bombardment. In addition, the surface of the ice may be quite irregular, increasing the effective area of the sample. Assuming either of these possibilities, the H density is such that reasonable amounts of hydrogen could then stick and migrate on the surface until encountering a CO_2 fragment (e.g., CO) and undergoing a reaction. Under these circumstances, H_2CO would be more readily formed than CH_3OH, and this is indeed the case as evidenced by XPS data which shows that after 6 hr of processing, H_2CO is approximately 3 times more abundant than CH_3OH. On the basis of the XPS results alone, it is not possible to say with certainty whether bulk or surface processes are responsible for the production of the secondary molecules.

Additional insight can be found in the time dependence of the gas phase concentrations measured by the mass spectrometer, and shown in Figure 5. As will be discussed later, the time response of the gas phase concentration for a particular molecule depends on the diffusion of the molecule through the solid CO_2 matrix. The general time response for CO, H_2CO, and CH_3OH show a very similar shape, but there are large differences between these molecules' response and that for O_2. We assume that the O_2 results from reactions between dissociated atomic O, and that the time dependence of the O_2 in the chamber depends on the diffusion of O in the bulk. This assumption is consistent with the mass spectrometer response since, once large-scale diffusion begins, the concentration of mass 32 increases much faster than that for mass 29 (corresponding to CO), indicating that the diffusion constant for the parent molecule of mass 32 must be larger, and that the size of the molecule should, therefore, be smaller.

If the molecules H_2CO and CH_3OH are formed in the bulk, it seems likely that the response of their mass spectrometer plots would vary from the smaller molecule CO. In fact, the general similarity with slight differences between the experimental responses for CO, H_2CO, and CH_3OH can be duplicated by assuming that the H_2CO concentration is related to that of CO by a factor f, and that the CH_3OH concentration is related to that of CO by f^2, where f is a small fraction. These factors can be explained if surface hydrogenation reactions are responsible for the conversion of CO into the other two molecules. The reaction rate will be set by the timescale in which the hydrogen samples the sites on the surface. Since two reactions are required to go from CO to H_2CO and then another two from H_2CO to CH_3OH the use of the factors f and f^2 is probably reasonable although simplistic. From this analysis, we believe that the CO and O diffuse to the surface at different rates and that, once on the surface, they either desorb or participate in reactions, subsequently producing the secondary molecules H_2CO and CH_3OH, and possibly O_2.

As stated earlier, it is evident from the XPS data that a cap of H_2O grows on the solid CO_2 during the X-ray photoprocessing. The obvious concern with such a result is the possibility that the H_2O just accretes from the vacuum. To that point, it is important to note that our experiments were performed in a stainless steel UHV chamber, which has a base pressure of $\sim 5 \times 10^{-10}$ T, and that this chamber was closed to the atmosphere, through the use of a load lock, for at least 6 months prior to the experiment. The partial pressure of H_2O in the chamber was small, and the dominant contaminant was hydrogen, as is typical in a UHV chamber. Despite this favorable situation, a control run under identical experimental conditions (but with the X-ray source turned off during the 5 hr experiment) was performed. The results are shown in Figures 4*a* and 4*b*. Although a small amount of H_2O does appear in the film after 5.2 hr of formation, as expected, it is at least 3 times less than the amount created in the processed case, indicating that X-ray induced photoprocessing events lead to the formation of H_2O either in or on the CO_2 film.

That the H_2O is almost certainly on the surface is strongly supported by two characteristics of the ice film's response to the X-ray photoprocessing. First, the total integrated intensity of the C 1*s* line decreases with time, as shown in Figure 6. This decrease could be due to the diffusion of photolyzed carbon-bearing molecules out of the ice, but the intensity of molecules other than CO_2 in the line suggest that this effect would not result in as large a reduction in the overall intensity of the line. It is much more likely that the H_2O, which shows dramatic increase with time from the O 1*s* spectra (Fig. 3*c*), is growing as a cap on the surface.

The second piece of evidence to support this contention comes from Figure 7, showing the O 1*s* spectra for a CO_2/H_2O ice, grown with an initial ratio of approximately 45:55. After 4.5 hr of processing, Figure 7*b* shows that the H_2O component in the ice has grown dramatically relative to the CO_2. The scale in each figure is normalizied to the highest peak, but the total integrated areas of each peak also support this conclusion. However, tabulating those numbers would be misleading; an increase of a surface component automatically decreases the subsurface intensity because the sampling depth remains relatively constant. Figure 7*c* shows that after sputtering the ice for 15 minutes with 4 keV Ar^+ ions the relative amounts of each constituent are once again about the same, confirming that the H_2O layer grows on the surface and, when combined with the other results, that the H_2O is photoproduced, with the con-

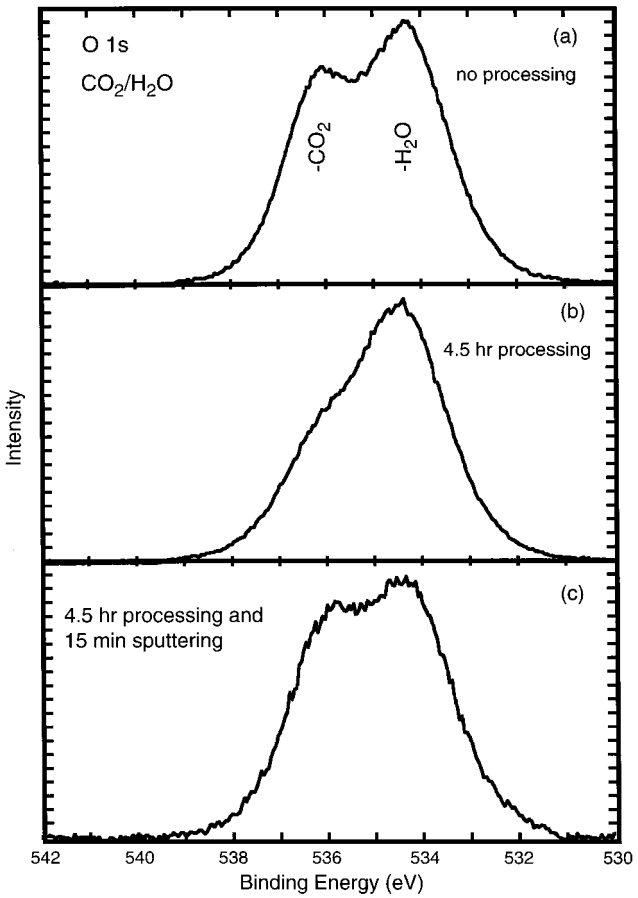

FIG. 7.—O 1*s* XPS line for CO_2/H_2O ice mixture: (*a*) as-grown ice, (*b*) after 4.5 hr of X-ray processing, and (*c*) after an additional 15 minutes of ion sputtering.

clusion that a surface reaction is responsible for the production of the H_2O.

Modeling done for gas-solid interactions (d'Hendecourt et al. 1985) shows that water producing reactions take place on the surface of grains in the interstellar medium. A gas-phase reaction producing additional H_2O, which then accretes on the surface, is possible but, as illustrated in Figure 5, the increase in mass 18 is too small to account for the difference in XPS intensity between the unprocessed (5.2 hr) film and the 6 hr processed film. A surface process involving O or O_2 trapped on the surface and reacting with hydrogen derived from the residual gas in the chamber is the most likely mechanism.

An estimate of the rate of this H_2O forming surface reaction can be found using the XPS data. Although the intensity of the H_2O line in the O 1*s* XPS spectra (Fig. 3) is an appreciable fraction of the CO_2 line, the O leading to H_2O formation can diffuse from the entire bulk of the ice while the XPS signal is derived from the topmost 50 to 100 Å. Therefore, a simple ratio of H_2O to CO_2 in the XPS line as a percentage of the total film converted to H_2O is not appropriate in this case. From Figure 6, the total integrated area of the C 1*s* line, which is dominated by CO_2, decreases from 15,000 to 9000 counts. Using a standard exponential decay for the core electron intensity of a film covered by a layer of absorbing material, in this case H_2O, for a take off angle of 45°, and using 40 Å as the inelastic mean free path for the photoelectrons in H_2O (as determined from the empirical formula derived by Tanuma, Powell, & Penn 1993), we calculate the thickness of H_2O to be 14 ± 4 Å after 6 hr of processing. Assuming a density for the H_2O of 1 g cm^{-3}, this thickness yields a growth rate of 2.6×10^{11} cm^{-2} s^{-1}. This rate is approximately 2.6×10^{-4} monolayers s^{-1}. As mentioned earlier, the rate for H impacting the surface is about the same order of magnitude. The rate of CO production calculated above was 0.054 $photon^{-1}$. For a flux of 6×10^{13} photons cm^2 s^{-1}, we then calculate an O production rate throughout the ice of 3.2×10^{12} s^{-1}. The number of O atoms on the surface at any one time due to diffusion will be much less. It is not clear whether the production rate of H_2O is limited by the supply of O or H to the surface. To probe this question as well as surface diffusion characteristics, measurements of the dependence of H_2O production on X-ray intensity, on the temperature of the ice and on the partial pressure of H in the chamber should be done. Some of these experiments will be attempted in the near future by this group.

While, until now, we have used the mass spectrometer data to simply confirm the presence of certain molecules evolving from the ice due to the X-ray photolysis, the behavior of the gas phase population as a function of time is, in itself, of interest. Once again, Figure 5 shows the relative concentrations of a set of selected masses in the chamber as a function of processing time. Only the most significant of a large number of masses monitored are presented in this figure. The general behavior of the mass concentration with time should be dependent on three things: the rate of production of molecules in the ice, the rate of diffusion of these molecules out of the ice, and the efficiency of the ion pump in removing these molecules from the chamber. The production rate is set by the flux of the X-ray source, which we assume to remain relatively constant during the experiment. Assuming that the ice is dominated by CO_2 throughout the entire experiment, the production rate for any measured species should remain constant. The diffusion rate should be dependent on the diffusing species, the solid matrix (in this case solid CO_2) and the temperature of the ice. The pumping speed shows a logarithmic dependence with pressure in the 10^{-10} T to 10^{-8} T region. Any simple diffusion model with a single diffusion constant for a given mass will show an immediate rise in the pressure in the chamber at time $t = 0$ since reactions and subsequent diffusion should occur as soon as the processing begins. However, the concentration of the masses we observed does not increase until after a long time delay of approximately 2500 s.

A similar delay has been seen in previous mass spectrometer work on ion processed ices (Pirronello et al. 1988). This delay cannot be understood under the constraints of a simple diffusion model, but other physical processes can perhaps account for it. One possibility is that most of the processing in the ice takes place at the ice/substrate interface and is due to secondary electrons produced in the stainless steel substrate by the X-ray flux. If this were the case, there would indeed be a time lag before any substantial increase in the gas phase concentrations. This lag would, however, be thickness dependent. For ices of various thickness, no clear dependence of the time lag on thickness was seen, although minor variations were observed. Consequently, this explanation was discarded.

Another possibility, suggested by Pirronello et al. (1988), is that the diffusion coefficients for the CO_2 fragments in the ice matrix are initially extremely small but that changes

occurring in the ice cause a sudden increase of several orders of magnitude in these coefficients. It is possible that disorder induced in the ice by the X-rays could be responsible for this postulated increase. Each incident photon has an energy greater than 1000 eV, while only several eV are needed to dissociate a CO_2 molecule. The difference in energy must be deposited into the ice. In this scenario, the disorder in the ice would increase until a percolation threshold of sorts was reached, after which the diffusion of small species such as CO and O would increase dramatically. The time lag under these conditions would not depend strongly on thickness but would show a dependence on other ice properties, such as density and temperature. The lag should also depend on X-ray flux. In future experiments, some of these dependencies will be investigated.

Even though a quantitative explanation of the time lag is possible, we cannot model the lag's duration. However, we can still gain some quantitative information about the diffusion properties of the dissociation products after the percolation event has taken place, by fitting the mass spectrometer data for the region after the time lag, which begins at about 2500 s. We see that once the diffusion starts in earnest, the concentrations of CO, O, CH_3OH, and H_2CO all rise, with one time dependence for O and one for CO, H_2CO, and CH_3OH. That this time development is dependent upon material can be seen in Figure 8, which shows the mass spectrometer data for a processed $^{13}CO_2/H_2O$ ice mixture. For this solid, the time response of the gas-phase concentrations is completely different than for the pure CO_2 ice.

To simulate the increase in concentration for the pure CO_2 ice, we designed a simple model. Assuming that the gas molecule can be created at any depth in the ice from 0 to 5500 Å (which is the thickness), the molecule can then begin to diffuse away from its creation point with some diffusion coefficient D. At some time later, the probability for the position of the molecule with respect to its starting point is represented by the surface of an expanding sphere. When this sphere intersects the plane ice-gas interface, the molecule escapes to the gas phase. The derivative of the modeled function was then taken to produce a rate, which was then convoluted with a step function, representing the status of the X-rays, off or on. This convoluted function was used as the source term in a first-order differential equation, where the pumping speed was represented by a logarithmic term, as discussed earlier.

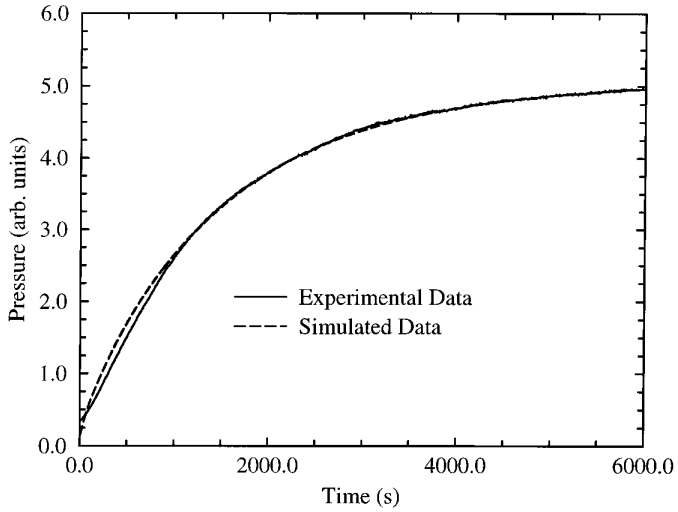

FIG. 9.—Evolution of pressure for O in X-ray–processed CO_2 ice for times beginning after sharp increase in diffusion rate. Results from the experiment and model are both shown. Best agreement is obtained for a diffusion constant of 5×10^{-12} cm^2 s^{-1}.

The equation was solved with one other parameter; the ratio between the beginning pressure and the final saturated pressure. The solution to this equation was scaled to meet the experimental results at 6000 s. It is noted that varying the diffusion coefficient changed the slope of the increasing region dramatically. Modeled functions with good agreement were produced for the two primary species in the ice, CO and O. Figure 9 is a plot of the experimental data for the O molecule in a nonisotopic CO_2 ice. The theoretical plot which shows the best agreement yields a diffusion coefficient of $(5 \pm 1) \times 10^{-12}$ cm^2 s^{-1}. In Figure 10, the model with the best agreement is shown for CO; the diffusion coefficient in this case is $(1 \pm 0.5) \times 10^{-12}$ cm^2 s^{-1}. We

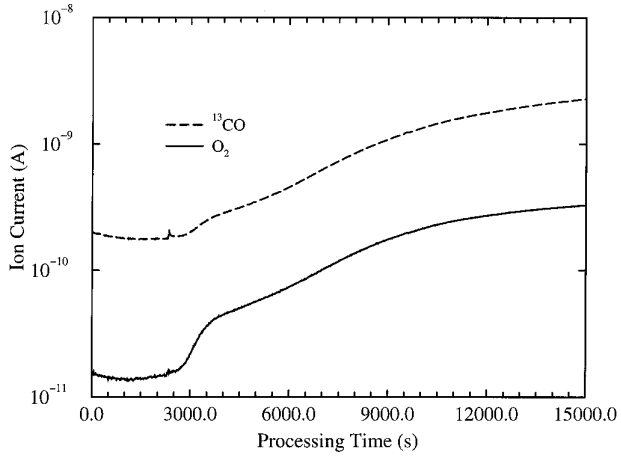

FIG. 8.—Time evolution of gas phase molecular concentrations for ^{13}CO and O_2 in a $^{13}CO_2/H_2O$ ice mixture, as a function of X-ray processing time.

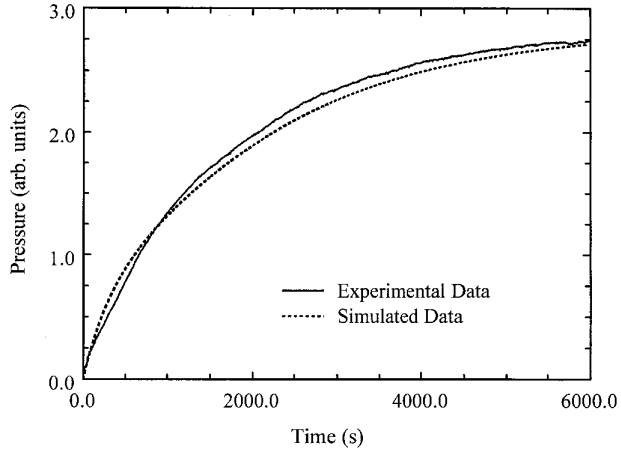

FIG. 10.—Evolution of pressure for CO in X-ray–processed CO_2 ice for times beginning after sharp increase in diffusion rate. Results from the experiment and model are both shown. Best agreement is obtained for a diffusion constant of 1×10^{-12} cm^2 s^{-1}.

were not able to match the data for the CO molecule as closely as for O and attribute this poorer reproduction to the simplicity of the model. We are now working on a more detailed model which hopefully will improve the agreement. The relative values for the coefficients lead to the conclusion that the diffusing oxygen-bearing species is smaller than CO, which supports the possibility of atomic O residing in the ice. Also, comparisons with studies of CO diffusion in H_2O (Sandford & Allamandola 1988), where a value for D of 2.8×10^{-14} cm^2 s^{-1} was measured at a temperature of 150 K, show that the diffusion coefficient in the X-ray–processed ice is 2 orders of magnitude larger, at a much lower temperature. This difference supports the contention that the diffusion in the X-ray–processed ices is enhanced by disorder in the CO_2. Even so, the measurement of the coefficients for this processed ice could be of use when simulating the effects of ice disorder on the gas-solid molecular abundance ratios.

As discussed earlier, the measured photoproduction rate for the CO molecule did not include amounts lost to the gas phase. We can now calculate an estimate for this amount using the diffusion model. The source term used in the differential equation represents the rate at which a molecule diffuses out of the film. If this term is integrated from 0 to 20,000 s, we will have an estimate for the total number of molecules per cm^3 which go into the gas phase. We estimated the volume of the chamber to be 60 liters, using simple geometry, with a large uncertainty of 20 liters. Assuming a uniform concentration in the chamber, the calculation yields 6×10^{14} molecules. This amount would add approximately 4.6×10^{-4} photon^{-1} to the photoproduction rate and, even though the uncertainties are up to 30%, does not change the overall production rate calculated earlier, on the basis of solid phase contributions alone, to be 5.4×10^{-2} photon^{-1}.

5. CONCLUSIONS

Films of CO_2 ice have been processed by X-ray irradiation and studied using XPS and mass spectrometry. The XPS results show that the CO_2 is photodissociated by the X-rays and that the products CO, O, H_2CO, CH_3OH and H_2O are created in the film. The photoproduction rate for the directly produced CO was measured to be 5.4×10^{-2} photon^{-1}, corresponding to a production cross section of 4.7×10^{-20} cm^2. From consideration of the XPS and mass spectrometer data, it is clear that the reactions producing the daughter molecules occur on the surface of the ice, and we infer that residual hydrogen from the vacuum chamber is responsible for the necessary hydrogenation reactions. For the case of the H_2O, the surface growth rate was calculated to be 2.6×10^{-4} monolayers s^{-1}.

The time development of the gas phase concentrations as measured by the mass spectrometer showed a large time lag which is attributed to a sudden change in the diffusion properties of the ice due to the creation of defects in the film by the excess energy deposited by the X-rays. Modeling the gas-phase concentrations of the dissociated molecules, the diffusion coefficients of O and CO in the solid CO_2 were found to be 5×10^{-12} cm^2 s^{-1} and 1×10^{-12} cm^2 s^{-1}, respectively.

We gratefully acknowledge the support of the NSF, DMR-9217526; NASA Origins of the Solar System, NAGW-4232; NASA Planetary Astronomy Program, NAGW-2811; and the NAU Organized Research program.

REFERENCES

Allamandola, L. J., & Sanford, S. A. 1988, in Dust in the Universe, ed. M. E. Bailey & D. A. Williams (Cambridge: Cambridge Univ. Press), 229
Allamandola, L. J., Sandford, S. A., Tielens, A. G. G. M., & Herbst, T. 1992, ApJ, 299, 134
Allamandola, L. J., Sandford, S. A., & Valero, G. J. 1988, Icarus, 76, 225
Benit, J., Bibring, J.-P., & Rocard, F. 1988, Nucl. Instrum. & Meth., B32, 349
Blake, G. A., Sutton, E. C., Masson, C. R., & Phillips, T. G. 1987, ApJ, 315, 621
d'Hendecourt, L. B., & Allamandola, L. J. 1986, A&AS, 64, 453
d'Hendecourt, L. B., Allamandola, L. J., & Greenberg, J. M. 1985, A&A, 152, 130
d'Hendecourt, L. B., Allamandola, L. J., Grim, R. J. A., & Greenberg, J. M. 1986, A&A, 158, 119
d'Hendecourt, L. B., & Jourdain de Muizon, M. 1989, A&A, 223, L5
de Grauw, T., et al. 1996, A&A, 315, L345
Feigelson, E. D., Casanova, S., Montmerle, T., & Guibert, J. 1993, ApJ, 416, 623
Gelius, U., Hedén, P. F., Hedman, J., Lindberg, B. J., Manne, R., Nordberg, R., Nordling, C., & Siegbahn, K. 1970, Phys. Scr., 2, 70
Gerakines, P. A., Schutte, W. A., & Ehrenfreund, P. 1996, A&A, 312, 289
Greenberg, J. M., Mendoza-Gomez, C. X., deGroot, M. S., & Breukers, R. 1993, in Dust and Chemistry in Astronomy, ed. T. J. Millar & D. A. Williams (Bristol: IOP Publ. Ltd.), 271
Gürtler, J., Henning, T., Kömpe, C., Pfau, W., Krätschmer, W., & Lemke, D. 1996, A&A, 315, L189
Hasegawa, T. I., Herbst, E., & Leung, C. M. 1992, ApJS, 82, 167
Herbst, E. 1993, in Dust and Chemistry in Astronomy, ed. T. J. Millar & D. A. Williams (Bristol: IOP Publ. Ltd.), 183
Hollenbach, D., & Salpeter, E. E. 1970, J. Chem. Phys., 53, 79
———. 1971, ApJ, 163, 155
Kopp, M., Barnall, D. E., & Lowe, I. J. 1965, J. Chem. Phys., 43, 2965
Lacy, J. H., Carr, J. S., Evans, N. J. H., Baas, F., Achtermann, J. M., & Arens, J. F. 1991, ApJ, 376, 556
Leitch-Devlin, M. A., & Williams, D. A. 1985, MNRAS, 213, 295
Moore, M. H., Donn, B., Khanna, R., & A'Hearn, M. F. 1983, Icarus, 54, 388
Moore, M. H., & Hudson, R. L. 1992, ApJ, 401, 353
Mumma, M. J., Weissman, P. R., & Stern, S. A. 1993, in Protostars and Planets, Vol. 3, ed. E. H. Levy & J. Lunine (Tuscon: Univ. Arizona Press), 117
Pirronello, V., Brown, W. L., Lanzerotti, L. J., & Maclennan, C. G. 1988, in Experiments on Cosmic Dust Analogues, ed. E. Bussoletti (Dordrecht: Kluwer), 287
Pirronello, V., Brown, W. L., Lanzerotti, L. J., Marcantonio, K. J., & Simmons, E. 1982, ApJ, 262, 636
Pirronella, V., Liu, C., Shen, L., & Vidali, G. 1997, ApJ, 475, L69
Sandford, S. A., & Allamandola, L. J. 1988, Icarus, 76, 201
———. 1990a, Icarus, 87, 188
———. 1990b, ApJ, 355, 357
Siegbahn, K., et al. 1969, ESCA Applied to Free Molecules (Amsterdam: North Holland)
Strauss, H. L., Chen, Z., & Loong, C.-K. 1994, J. Chem. Phys., 101, 7177
Tanuma, S., Powell, C. J., & Penn, D. R. 1993, Surface and Interface Analysis, 21, 165
Tielens, A. G. G. M. 1992, in Chemistry and Spectroscopy of Interstellar Molecules, ed. D. K. Bohme, E. Herbst, N. Kaifu, & S. Saito (Tokyo: Univ. Tokyo Press), 237
Tielens, A. G. G. M., & Hagen, W. 1982, A&A, 114, 245
Tielens, A. G. G. M., Tokunaga, A. T., Geballe, T. R., & Baas, F. 1991, ApJ, 381, 181
Turner, B. E. 1990, ApJ, 362, L29
Williams, D. A. 1993, in Dust and Chemistry in Astronomy, ed. T. J. Millar & D. A. Williams (Bristol: IOP Publ. Ltd.), 143
Woodruff, D. P., & Delchar, T. A. 1994, Modern Techniques of Surface Science (2nd ed.: Cambridge: Cambridge Univ. Press)